Contents lists available at ScienceDirect

International Journal of Mechanical Sciences

Theoretical analysis of the acceleration effect of the magnetic field on the shaped charge jet

Bin Ma [a,b], Zhengxiang Huang [a,*], Zhongwei Guan [b], Xin Jia [a], Qiangqiang Xiao [a], Xudong Zu [a]

[a] School of Mechanical Engineering, Nanjing University of Science and Technology, Nanjing 210094, PR China
[b] School of Engineering, University of Liverpool, Liverpool L69 3GQ, UK

ARTICLE INFO

Keywords:
Shaped charge jet
Magnetic field
Acceleration, X-ray

ABSTRACT

This work analyzes the magnetic field produced by the solenoid and its acceleration effect on a shaped charge jet (SCJ) with the radial component of the field being considered. A theoretical model was developed to analyze the acceleration mechanism of the field on the SCJ. The results show that the axial velocity of the jet particles can be increased due to the existence of the magnetic field produced by the solenoid. In addition, the related X-ray experiments were conducted to verify the theory. The theoretical results correlate with the experimental results reasonably well.

1. Introduction

Shaped charge jets (SCJs) are used extensively in many industrial sectors, including petroleum and defense ones because of their significant penetration capability. The velocity of the jet tip can reach 6000–8000 m/s, even up to 10,000 m/s, with the tail element flying at a velocity of approximately 2000 m/s. The SCJ can experience considerable stretching at a strain rate ranging from 10^4 to 10^5 s^{-1} [1]. However, the SCJ becomes unstable and breaks up into many pieces with approximately equal size for a certain length of time (Breakup time) [2,3]. After breakup of a SCJ, the particles do not remain aligned with the SCJ axis, instead of starting rotation [4]. The breakup and the rotation after breakup of the SCJ can significantly degrade the performance of the SCJ. Based on the related penetration theory of the SCJ, the increase of the jet velocity is beneficial to improve the penetration ability of the SCJ [5,6]. In the past a few decades, some scholars devoted themselves to improve the penetration ability of SCJs. Previous methods mainly focus on improving the physical–mechanical properties of SCJ materials and the machining process, as well as optimizing the shape and size of liners. However, the current penetration capability of SCJs still cannot satisfy the practical requirements.

Previous studies showed that the penetration capability of shaped charges could be improved by electromagnetic actions. Littlefield [2] theoretically analyzed the stability of rapidly stretching and perfectly plastic jets when they were subjected to axial magnetic fields. In his study, the jet was assumed to be uniformly elongated, infinitely long and isothermal. Linear perturbation theory was also employed to calculate the time evolution of small disturbances. The results indicated that the axial magnetic field imposed on the SCJ could effectively inhibit the growth rates of perturbation. Fedorov et al. [7–9] and Babkin et al. [10] showed that jet stretching with a diffused magnetic field is accompanied by magnetic field compression inside the jet, thereby generating radial stretching electromagnetic forces. In their studies, an increase of 10% in the depth of penetration (DOP) was obtained when the magnetic induction intensity was changed from 1 Tesla to 10 Tesla. The authors then introduced several types of electromagnetic actions controlling the jet at different stages of shaped charge firing. They considered the salient deformation features of metal cumulative jets in a longitudinal low-frequency magnetic field based on a model of a uniformly stretching cylindrical incompressible rigid-plastic conducting rod. Ma et al. [11–17] analyzed the coupling process between the external magnetic field and the SCJ. They explored the inhibiting effect of the electromagnetic force on rotational motion of particles after the breakup of the SCJ. Their numerical simulations and theoretical models were verified by the corresponding experiments.

Although the coupling mechanisms between the SCJ and the magnetic field were extensively studied, the magnetic field produced by the solenoid was only regarded as a longitudinal field. As the results, the radial component of the field was neglected.

In this work, the magnetic field produced by the solenoid was analyzed by considering both the longitudinal and radial components of the field. Based on the Gauss's law, the expression of the radial component of the magnetic field was proposed. Following the law of electromagnetic induction, the electromagnetic force of the SCJ with the overall influence of the magnetic field was analyzed. Therefore, a comprehensive theoretical model was developed to describe the acceleration

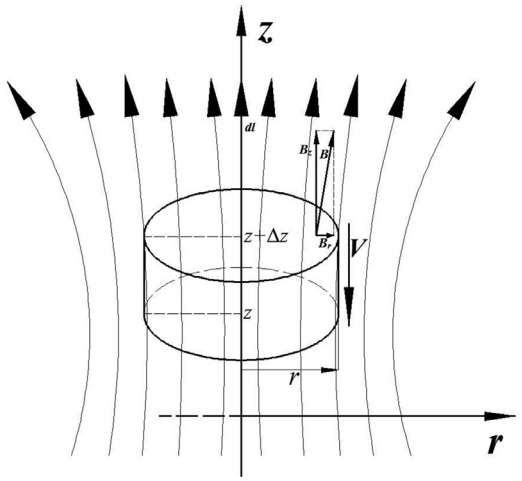

Fig. 1. Model for acceleration of a shaped charge jet element inside the external magnetic field.

mechanisms of the SCJ in the magnetic field. In addition, the X-ray experiments were conducted to verify the theoretical predictions.

2. Acceleration model of the SCJ inside the axial magnetic field

2.1. Analysis of the magnetic field produced by the solenoid

For the convenience of discussion, a cylindrical coordinate system is used, as shown in Fig. 1. The axis of the solenoid is set to z-axis, and the radial direction is r-axis. For a magnetic field B produced by a finite long solenoid, there are two components: the radial one B_r and the axial one B_z. The field is variable along the z direction. In fact, it gradually grows stronger from the entrance of the solenoid to the neutral position of the axis, then becomes weaker after passes the neutral position.

Since the magnetic field is passive, the net flux of the magnetic field out of any volume of the jet element is zero. Based on the magnetic version of Gauss's law, we can obtain [18]:

$$\nabla \cdot B = 0 \tag{1}$$

According to Fig. 1, there is [19]:

$$\pi r^2\left(-B_z(z) + B_z(z+dz)\right) + 2\pi r B_r \Delta z = 0 \tag{2}$$

Thus, according to Eq. (2), the relationship between B_r and B_z can be obtained as:

$$B_r = -\frac{r}{2}\frac{\partial B_z}{\partial z} \tag{3}$$

2.2. Force model of the SCJ inside the external magnetic field

For simplicity, it is assumed that: (1) the field is considered to be strictly symmetric about the z axis, (2) the component B_r is concentrated on the surface of the SCJ, (3) During the calculation of the magnetic induction imposed on the jet element, the motion of the jet element in the magnetic field is regarded as the uniform one and (4) air resistance and gravity are ignored.

According to the law of electromagnetic induction, the following relation can be obtained:

$$E \cdot 2\pi r = -\frac{d\phi}{dt} \tag{4}$$

here, E is the electric field induced, $\emptyset$ is the magnetic flux, and t is time.

The coupling process of the SCJ includes two stages, the first one is from the SCJ beginning to enter the solenoid to the moment of the external magnetic field diffusing into the SCJ completely; the second one begins from the end of the first stage to the jet leaving the solenoid.

However, the SCJ is only accelerated in the first stage rather than the second stage. At the first one, the variation of the magnetic flux is mainly caused by the change of both the cross-section of the SCJ and the magnetic induction intensity produced by the solenoid. Therefore, it arrives:

$$\frac{d\phi_1}{dt} = B_1\frac{dS_1}{dt} + S_1\frac{dB_1}{dt} \tag{5}$$

Where $\emptyset_1$ is the magnetic flux, B_1 is the magnetic induction intensity produced by the solenoid, and the S_1 is the cross-section of the SCJ at the first stage.

A low-frequency field can be diffused into the SCJ material and result in a "freezing effect" as mentioned in Refs. [7–9,20]. The time of magnetic field diffusing into the jet material can be calculated as 10.5 μs for the front-end of the SCJ according to the theory in Ref. [7], when the front-end of the SCJ has reached the initial position of the second stage at this moment. Therefore, at the second stage, the magnetic flux is constant due to the freezing effect of the magnetic field, i.e.

$$\phi_2 = \int B_2 dS_2 = C \tag{6}$$

here, $\emptyset_2$ is the magnetic flux, B_2 is the magnetic induction intensity inside the SCJ, the S_2 is the cross-section of the SCJ at the second stage, and C is a constant.

Combining Eqs. (4) and (6), the induced electric field inside the SCJ can be obtained as.

$$E_2 = 0 \tag{7}$$

Here, E_2 is the electric field induced at the second stage.

According to the result from Eq. (7), it is clearly that it has no action of electromagnetic force on the front-end of the SCJ, so that the SCJ cannot be accelerated at the second stage due to the freezing effect.

Based on the assumption of volume conservation [10], the radial velocity on the surface of the shaped charge jet can be obtained as:

$$V_r = -\frac{\dot{\varepsilon}_0 r_0}{2(1+\dot{\varepsilon}_0 t)^{\frac{3}{2}}} \tag{8}$$

The relationship between the initial radius r_0 and the current radius r of the shaped charge jet can be expressed as follows.

$$r = \frac{r_0}{\sqrt{1+\dot{\varepsilon}_0 t}} \tag{9}$$

Here, $\dot{\varepsilon}_0$ is the initial strain rate.

Combining Eqs. (4)–(9), the induced electric field due to the magnetic field coupling with the shaped charge jet can be expressed as:

$$E = \frac{B\dot{\varepsilon}_0}{2}\frac{r^3}{r_0^2} - \frac{r}{2}V_z\frac{\partial B}{\partial z} \tag{10}$$

Considering the differential form of the Ohm's law [7], the induced electric field can be also written as:

$$E = \eta j \tag{11}$$

Where η is the resistivity of the SCJ material and j is the density of the induced currents.

Based on Eqs. (10) and (11), the density of the current induced can be obtained during the magnetic field coupling with the SCJ.

$$j = \frac{B\dot{\varepsilon}_0}{2\eta}\frac{r^3}{r_0^2} - \frac{r}{2\eta}V_z\frac{\partial B}{\partial z} \tag{12}$$

Due to the skin effect [21], the induction current can be assumed to mainly act on the surface of the SCJ. Therefore, the induction current on the cross section of the SCJ can be considered as a circular current loop with a radius r, located in the magnetic field produced by the solenoid.

Based on the above assumption, the force on the jet element can be expressed as follows.

$$F = 2\pi r I B_r \tag{13}$$

Here, I is the induced current focusing on the surface of the SCJ due to the electro-magnetic induction.

Substituting Eq. (12) into Eq. (13), the axial electromagnetic force of the jet element in the first stage can be rewritten as

$$F = \frac{\pi r^2 l}{2}\frac{\partial B_z}{\partial z}\left(\frac{B\dot{\varepsilon}_0}{\eta}\frac{r^3}{r_0^2} - \frac{r}{\eta}V_z\frac{\partial B}{\partial z}\right) \tag{14}$$

Furthermore, the acceleration of the SCJ can be linked to the electromagnetic force on the basis of the Newton's Second Law.

In addition, the mass of the jet element can be calculated using Eq. (15) below.

$$m = \rho\pi r^2 l \tag{15}$$

Therefore, the acceleration of the jet element due to the presence of the magnetic field produced by the solenoid can be given as:

$$a = \frac{1}{2\rho}\frac{\partial B_z}{\partial z}\left(\frac{B\dot{\varepsilon}_0}{\eta}\frac{r^3}{r_0^2} - \frac{r}{\eta}V_z\frac{\partial B}{\partial z}\right) \tag{16}$$

The acceleration of the jet element at any position within the solenoid can be calculated using Eq. (16). In order to have the experimental verification, the ultimate velocity of the jet element needs to be obtained. Therefore, the average acceleration of the jet element is obtained from the displacement integration of Eq. (16), i.e.

$$a_{ave} = \frac{\int_0^{z_e} a\,dz}{z_e} \tag{17}$$

Here, z_e is the coordinate of the exit of the solenoid.

The average acceleration a_{ave} is considered as a constant to describe the acceleration process of the jet element during its passing through the solenoid. The acceleration process of the SCJ caused by the electromagnetic force is complex. Thus the motion of the jet element in the magnetic field can be regarded as the uniformly accelerative one when the ultimate velocity of the SCJ is calculated. The ultimate velocity of the jet element can be expressed as

$$v_{ul} = v_0 + a_{ave}t \tag{18}$$

Where t is the acceleration time of the SCJ due to the existence of the magnetic field; v_0, v_{ul} are the velocities of the SCJ entering the solenoid and its ultimate velocity, respectively.

3. Results and discussion

3.1. Parameters of the SCJ

In this work, X-ray experiments were conducted to obtain the SCJ parameters to be used in the calculations. The relative position of the experimental setup in X-ray experiments is the same as DOP experiments mentioned in Ref. [22]. The experimental results are shown in Fig. 2. The first X-ray image (Marked I) was captured at 160 μs, which was used to show the shape of the SCJ produced and stretched without the influence of magnetic field. The other three images (Marked as II, III and IV) were obtained at the time intervals of 152, 160 and 192 μs respectively, which were used to obtain parameters of the SCJ used in theoretical calculations. Based on the X-ray experimental results, the average diameter of the front-end of the SCJ is 4.16 mm, and its average length is 13.1 mm. Also, the initial strain rate is 3.05×10^5 s^{-1} and the initial diameter of the front-end of the SCJ is 4.28 mm [16].

3.2. Characteristics of the discharge current and magnetic induction

The discharge voltage at both ends of the capacitor is 20.18 kV. According to the electrical parameters shown in Table 1 and the theoretical analysis for the circuit mentioned in Refs. [14–16], the analytical results of the discharge current can be obtained. The results obtained from the experiments and theoretical calculations are shown in Fig. 3, which indicate reasonably good correlation, especially for the first half.

Table 1
The related electrical parameters.

Name of elements	Electrical parameters		
	Induction/μH	Resistance/mΩ	Capacitance/μF
Capacitors	–	–	77.9
Solenoid	7	5.1	–
Connecting wire	53.6	92	–

In fact, the experimental discharge current is consistent with the theoretical calculations before 300 μs, except for the initial stage. In addition, some variations between the theoretical and the experimental results of the discharge current appear with the passage of time. The reasons for the discrepancies may be listed as follows.

(1) The missing signal in the initial stage was caused by the high trigging level of the oscilloscope. However, if the trigging level was low, the oscilloscope would be trigged by an interference signal from the environment. For the circuit, the discharge current is impossible to have mutation from zero. Thus, the discharge current signal from experiments is normal;
(2) The sensitivity of the measuring equipment is low;
(3) The state of the electrical conductors in the theoretical calculations was not completely consistent with the experiments.

Based on the analysis of the magnetic field and the solenoid parameters mentioned in [16], the magnetic induction intensity can be calculated when a jet element arrives at any position in the solenoid. The calculation results are displayed in Fig. 4.

According to the calculation results, the magnetic induction intensity is more than 1 Tesla through almost the whole process because of the reasonable timing, and an appropriate timing can help optimize the use of the magnetic field produced by solenoid. However, the external magnetic field is always changing with time in experiments. In order to quantitatively assess the magnetic field in the coupling process, we calculate only the average magnetic induction intensity of the jet front-end experiencing through the integral. The result of the average magnetic induction is 1.45 Tesla.

3.3. Analysis of acceleration

According to the theoretical analysis of the discharge current and the experimental results, the evolution of the magnetic field of the jet front-end can be evaluated. For the SCJ parameters given above, the acceleration caused by electromagnetic force can be calculated according to Eq. (17), as shown in Fig. 5.

According to Fig. 5, it is clear that the acceleration due to the effect of the magnetic field increases initially, then decreases gradually until the acceleration value approaches zero. Firstly, based on the characteristics of the magnetic field produced by the solenoid, the radial component of the magnetic induction gradually decreases to zero from the entrance of the solenoid to the central position of the axis of the solenoid. Secondly, the cross-section of the SCJ element gradually decreases, which could lead to the rise of the magnetic induction intensity inside the SCJ. In the early stage, the rise of the magnetic induction intensity, which is caused by the decrease of the cross-section of the SCJ, is a predominant factor. Then, the decline of the radial component of the magnetic induction is beyond the rise of the magnetic induction intensity caused by the decrease of the cross-section gradually, and becomes a dominate factor. It is the above reasons that lead to increase the acceleration of the jet front-end, and then decrease.

From Fig. 5, one can obtain the acceleration at the front-end of the SCJ when it arrives at any position along the axis of the solenoid. However, it is necessary to determine an overall acceleration to assess the effect of the magnetic field on the velocity of the jet front-end. This overall acceleration can be calculated by using Eq. (17), which

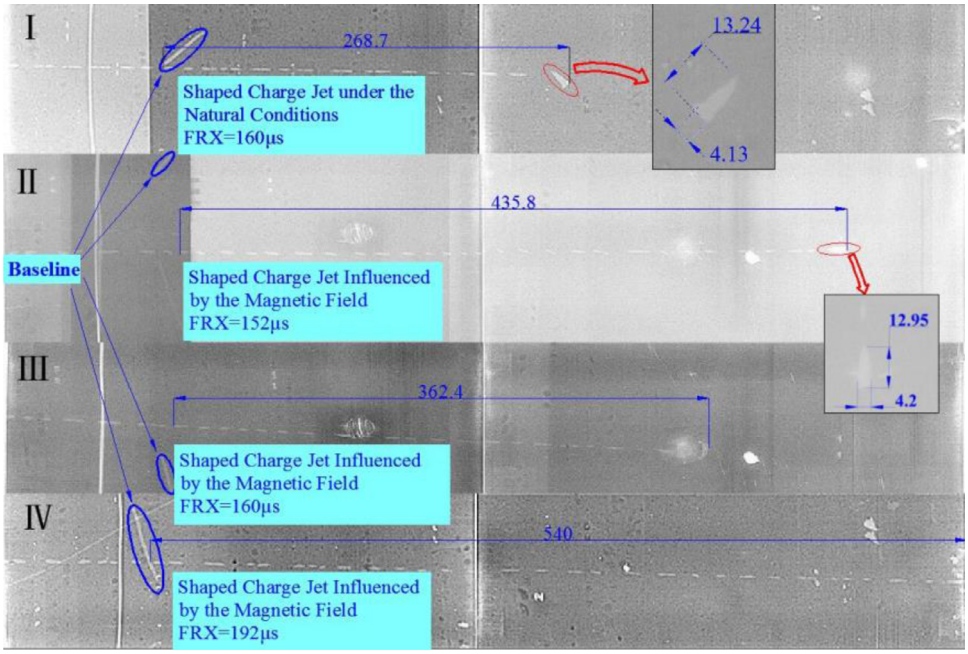

Fig. 2. X-ray images of the shaped charge jet.

Table 2
Experimental and theoretical results.

NO.	B/Tesla	Experimental velocity leaving the solenoid /mm μs^{-1}	Theoretical velocity leaving the solenoid / mm μs^{-1}	Error of increment /%
1	1.45	7.14	6.52	9.5
2		6.33		2.9
3		6.20		4.9

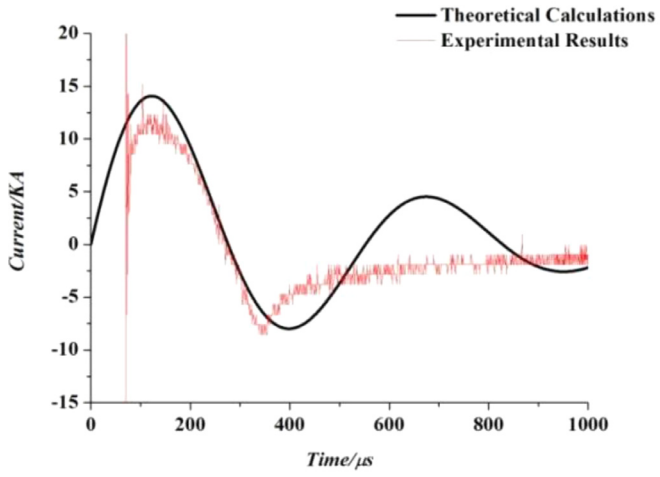

Fig. 3. Discharge current of dynamic experiments in case of $U_0 = 20.18$ *kV*.

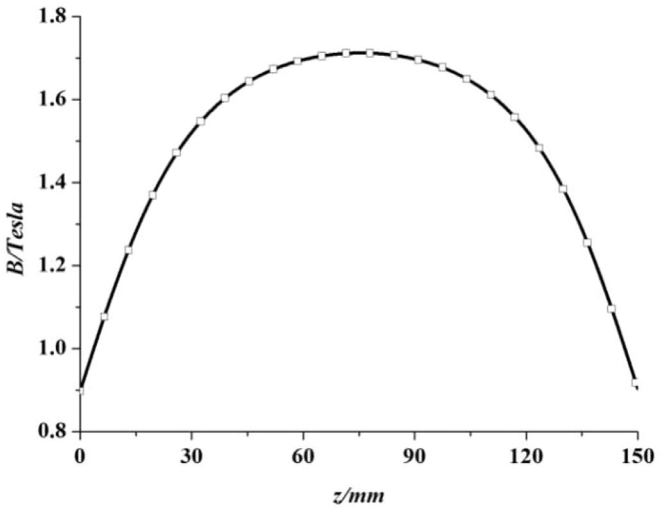

Fig. 4. Evolution of magnetic induction intensity of the element reaching different positions of the solenoid axis.

is 0.0214 mm μs^{-2}. Based on the structure of the solenoid introduced in Ref. [16], the span of the winding coils of the solenoid is 150 mm, namely, $z_e = 150$ mm. Combining the Eq. (18) with the related parameters, the velocity of the front-end of the SCJ left the solenoid can be calculated, which is shown in Table 2.

In order to verify the validity of the theoretical analysis, the experimental results are shown in Fig. 2. In the experiments, the bottom of the liner is used as a reference point, and the moment of the jet tip reaching the bottom of the shaped charge liner is set as zero time. The distance between the bottom of the liner and the baseline marked in the X-ray image is 650 mm. For the experimental results, Marked I is captured at 160 μs, which is used to collect the shape of the SCJ without the influence of magnetic field. Marked II, III and IV are exposed at 152, 160and 192 μs, which are used to obtain the SCJ form in the existence of the strong magnetic field and to compare with those without the influence of magnetic field. It needs to note that the front-end of the SCJ flied out of the range of the image marked IV. Therefore, it assumes that the jet front-end just went out the range of the image marked IV during processing, which might lead to deviation, but could indicate the axial velocity of the SCJ was increased due to the action of the field in some

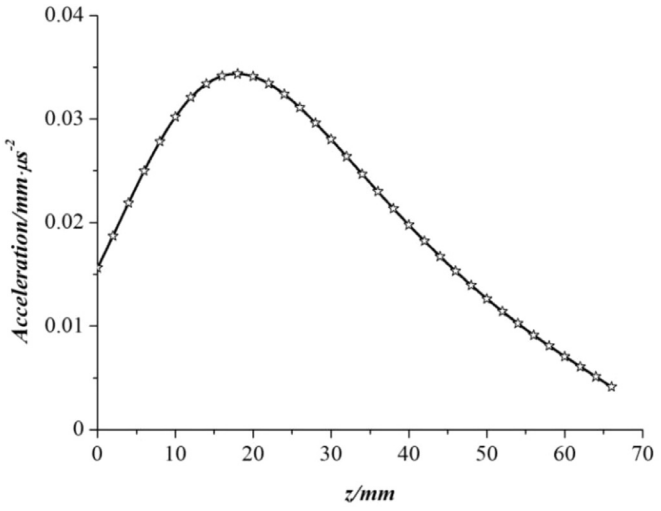

Fig. 5. Acceleration of the jet front-end caused by the electromagnetic force.

degree. Under the effect of the magnetic field, the average velocity of the SCJ front-end can be calculated based on the measured parameters. In addition, the velocity of the jet front-end after 160 μs (Marked I in Fig. 2) is 5.74 mm μs^{-1}without the influence of magnetic field. Due to the existence of the magnetic field, the velocities of the jet front-end are 7.14, 6.33 and 6.20 mm μs^{-1} at three moments (152, 160 and 192 μs), respectively. By comparison, the velocity of the SCJ front-end (the average of three experimental results) is increased by 14.2% under the effect of the external magnetic field.

According to the experimental results from Table 2, there are some variations for the results from the three experiments. The reasons for the variations may be: (1) the air resistance to the SCJ is ignored for simplifying the analysis; (2) the stability of each shaped charge used in the experiments cannot possibly be completely consistent, even for a precision shaped charge.

4. Conclusions

The magnetic field produced by the solenoid was analyzed by considering both the longitudinal and radial components. The current induced inside the SCJ was due to the existence of the longitudinal component, then the axial electromagnetic force was generated under the action of the radial component of the field. With the effects of the two components of the field, the SCJ could be further accelerated. Base on the research output presented above, the following conclusions may be drawn:

(1) A theoretical method, which was used for describing the acceleration effect of the magnetic field produced by solenoid on the shaped charge jet, was developed. Based on the model, we analyzed the acceleration of the front-end of the SCJ produced by Ø56 mm shaped charge.

(2) The velocity of the jet front-end after 160 μs is 5.74 mm μs^{-1} without the influence of magnetic field, and the theoretical velocity of the jet front-end with the field is 6.52 mm μs^{-1}. Therefore, the velocity of the SCJ front-end is increased by 13.6% due to the effect of the external magnetic field, which is beneficial to increasing the depth of penetration of the SCJ.

(3) The related experiments were conducted to verify the theoretical validity. The results showed that the velocities of the jet front-end are 7.14, 6.33 and 6.20 mm μs^{-1} at three different moments (152 μs, 160 μs and 192 μs), whilst the theoretical velocity due to the existence of magnetic field is 6.52 mm μs^{-1}. By comparison, the errors are 9.5%, 2.9% and 4.9% for the three experiments, respectively, which provides a reasonable support to the current theory.

Acknowledgements

This research is supported by the National Natural Science Funds for Distinguished Young Scholar of China [Grant No. 11602110] and the Natural Science Foundation of China [Grant No. 11272157]. The author Bin Ma thanks China Scholarship Council for supporting his study in University of Liverpool, UK.

Also, the authors are grateful to Prof. Hui Yu for her suggestions on the theory development.

References

[1] Jia X, Huang Z, Zu X, Gu X, Xiao Q. Theoretical analysis of the disturbance of shaped charge jet penetrating a woven fabric rubber composite armor. Int J Impact Eng 2014;65:69–78.
[2] Littlefield DL. Enhancement of stability in uniformly elongating plastic jets with electromagnetic fields. Physics Fluids A: Fluid Dynamics 1991;3:2927–35 1989-1993.
[3] Chou PC, Carleone J. The stability of shaped-charge jets. J Appl Phys 1977;48:4187–95.
[4] Rottenkolber E, Arnold W. Rotation rates and lateral velocities of shaped charge jet particles caused by breakup. In: Proceedings of the Fifteenth International Symposium on Ballistics, Australia; 2004.
[5] Schwartz W. Modified SDM model for the calculation of shaped charge hole profiles. Propellants, Explosives, Pyrotechnics 1994;19:192–201.
[6] Chou PC, Flis WJ. Recent developments in shaped charge technology. Propellants, Explosives, Pyrotechnics, 1986;11:99–114.
[7] Fedorov SV, Babkin AV, Ladov SV. salient features of inertial stretching of a high-gradient conducting rod in a longitudinal low-frequency magnetic field. J. Eng Phys Thermophys 2001;74:364–74.
[8] Fedorov SV, Babkin AV, Ladov SV, Shvetsov GA, Matrosov AD. Possibilities of controlling the shaped–charge effect by electromagnetic actions. Combust, Explos Shock Waves 2000;36:792–808.
[9] Fedorov S. Magnetic-field amplification in metal shaped-charge jets during their inertial elongation. Combust, Explos Shock Waves 2005;41:106–13.
[10] Babkin AV, Ladov SV, Marinin VM, Fedorov SV. Characteristics of inertially stretching shaped-charge jets in free flight. J Appl Mech Tech Phys 1997;38:171–6.
[11] Ma B, Huang Z, Zu Z, Xiao Q, Jia X. Experimental investigation and numerical simulationon magnetic field inhibiting rotation of shaped charge jet particle. J Ballistics 2015;27:77–83.
[12] Ma B, Huang Z, Zu X, Xiao Q, Jia X. Experimental Study of Magnetic Field Inhibiting Rotation of Shaped Charge Jet Particles. In: Woodly C, Cullis DI, editors. 29th International Symposium on Ballistics; 2016. p. 1322–9.
[13] Ma B, Huang Z, Zu X, Jia X, Xiao Q. Research on Magnetic Field Inhibiting the Rotation of Shaped Charge Jet Particles. Acta Armamentarii 2016;37:603–11.
[14] Ma; B, Huang; Z, Zu; X, Xiao; Q, Jia X. Theoretical and experimental study on the effect of the external strong magnetic field on the shaped charge jet. Modern Phys Lett B 2017;31:1750018.
[15] Ma B, Huang Z, Zu X, Xiao Q, Jia X. Influence of a longitudinal magnetic field on the coefficient of ultimate elongation of shaped charge jet. Explos Shock Waves 2016;36:1–8.
[16] Ma B, Huang Z, Zu X, Xiao Q. Experimental study on external strong magnetic fields coupling with the shaped charge jet. Int J Impact Eng 2016;98:88–96.
[17] Ma B, Huang Z, Zu X, Xiao Q, Jia X. Effect of time-sequence control on coupling of strong magnetic field and shaped charge jet. Acta Armamentarii 2016;37:2177–84.
[18] Landau LD, Bell J, Kearsley M, Pitaevskii L, Lifshitz E, Sykes J. Electrodynamics of continuous media. elsevier; 2013.
[19] Purcell EM, Morin DJ. Electricity and magnetism. Cambridge University Press; 2013.
[20] Shvetsov GA, Matrosov AD, Fedorov SV, Babkin AV, Ladov SV. Effect of external magnetic fields on shaped-charge operation. Int J Impact Eng 2011;38:521–6.
[21] Altgilbers LL, Grishnaev I, Smith IR, Tkach Y, Brown MD, Novac BM, et al. Magnetocumulative generators. In: Magnetocumulative generators. Springer; 2000. p. 57–123.
[22] Ma B, Huang Z, Xiao Q, Zu X, Jia X, Ji L. Effect of external magnetic field loaded at the initial period of inertial stretching stage on the stability of shaped charge jet. IEEE Trans Plasma Sci 2017;45:875–81.